

Early Pleistocene aridification of the Eastern Taurides, Turkey revealed by (U-Th)/He ages of supergene Attepe iron deposits

D. Currie¹, S. Keskin², and F. M. Stuart¹

¹ Isotope Geosciences, Scottish Universities Environmental Research Centre, Rankine Avenue, East Kilbride G75 0QF, UK.

² General Directorate of Mineral Research and Exploration, Eastern Black Sea District Office, Trabzon, Turkey.

Contents of this file

Introduction
Figures S1 to S10
Table S1

Introduction

Supporting information provided allows the reader further insight into where samples were collected from in relation to Earth's surface and what these samples look like in hand sample (Figures S1-S5). Following this, a general guide to each geological formation and their relation to ore mineralisation is provided in a stratigraphic column whilst cross sections are provided to give a sense of scale of each ore deposit (Figures S6-S7). To back up finer mineralogical insight discussed in the main text, diffractograms used to determine mineral phases present in each sample are given (Figure S8) as well as data gathered from the same analysis then processed to calculate crystallite size of each sample using the Scherrer equation (Table S1). Finally, plots of sample age against eU, crystallite size, and mineralogy are provided to back up suggestion in main text that no relationship between these aspects was noted (Figures S9-S10).

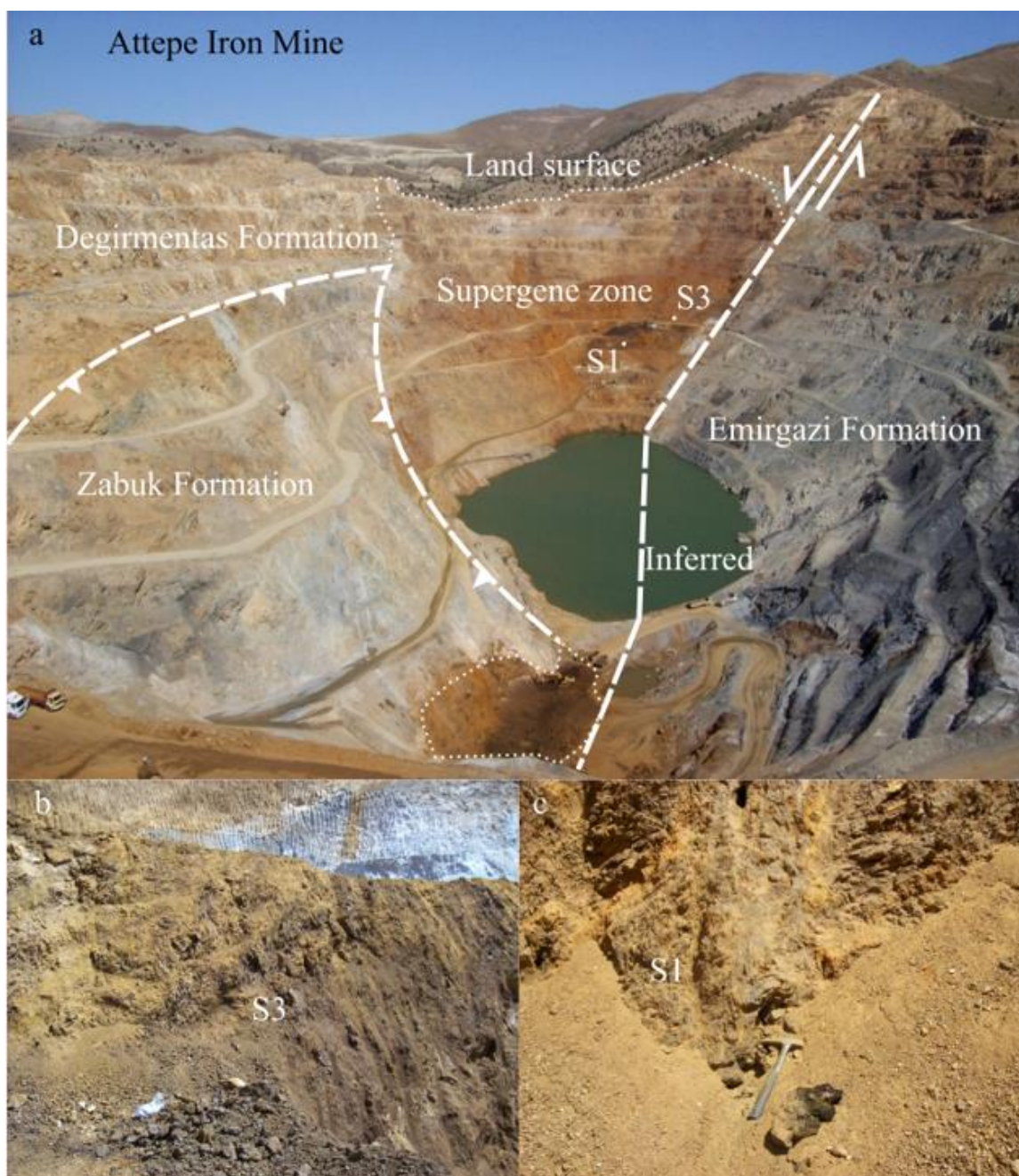


Figure S1. Field images of Attepe iron mine. A) view of the open pit mine. B) location of sample S1. C) location of sample S3.

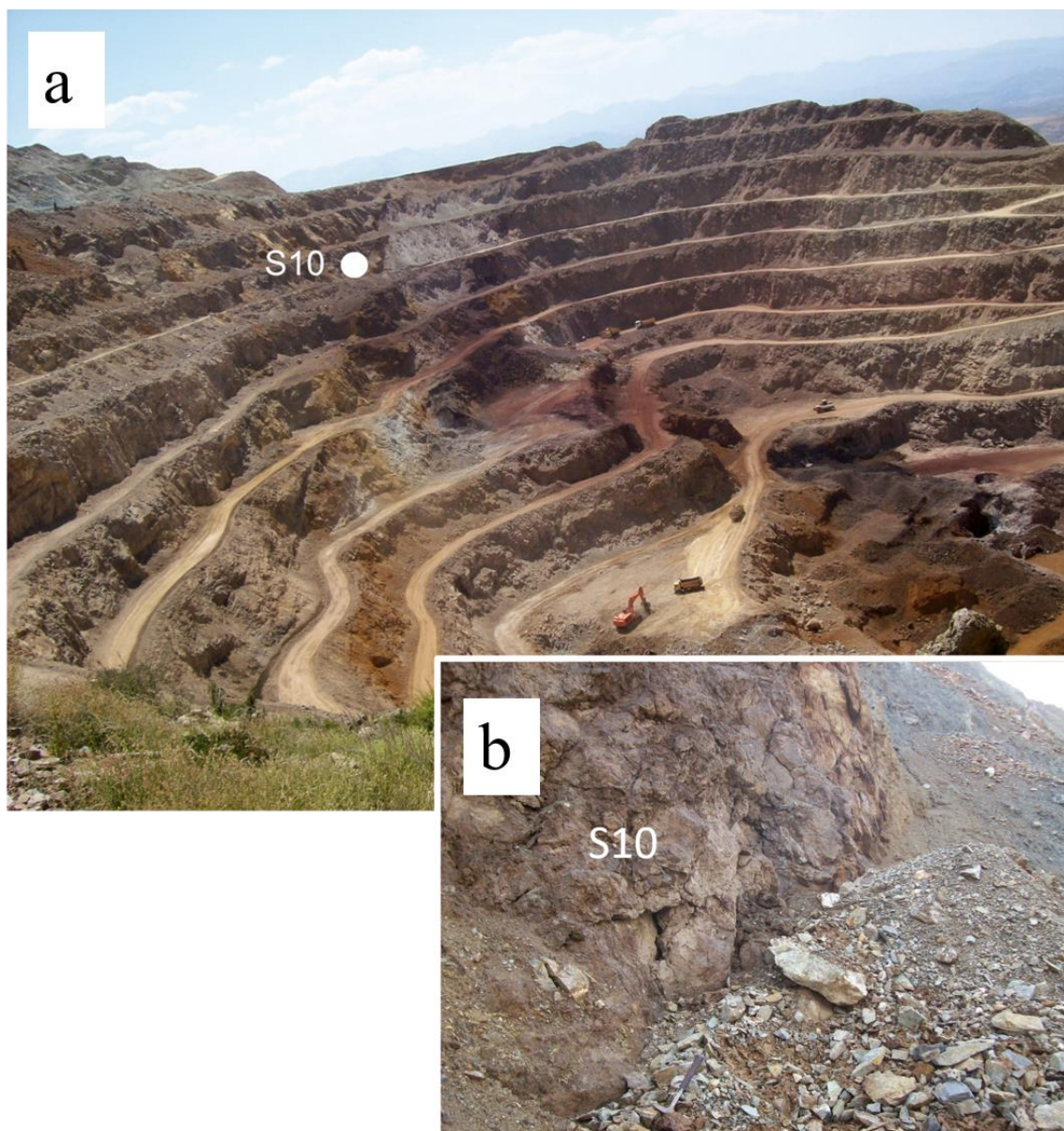


Figure S2. Field images of Karacat iron mine A) and B) the location of sample S10.

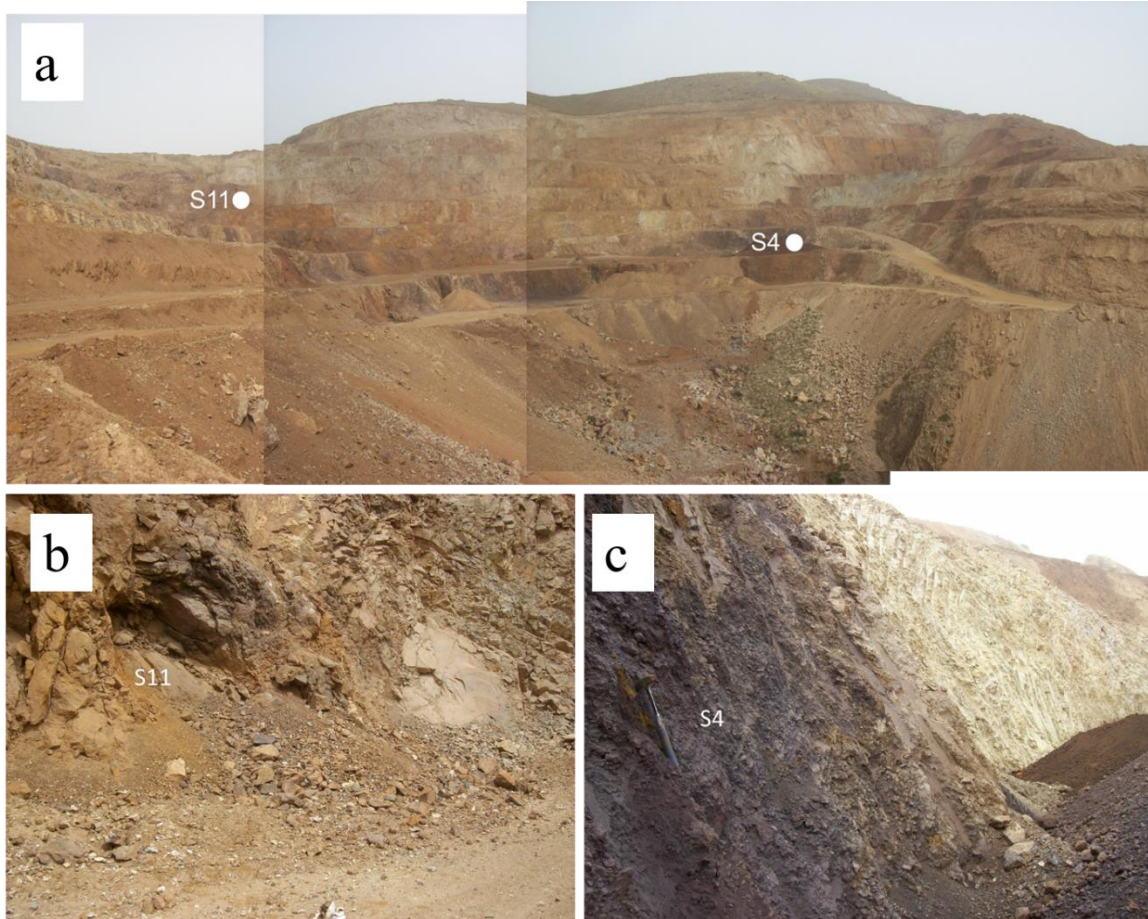


Figure S3. Field images of Elmadagbeli iron mine showing the open pit mine A) and the location of samples S11 (B) and S4 (C).

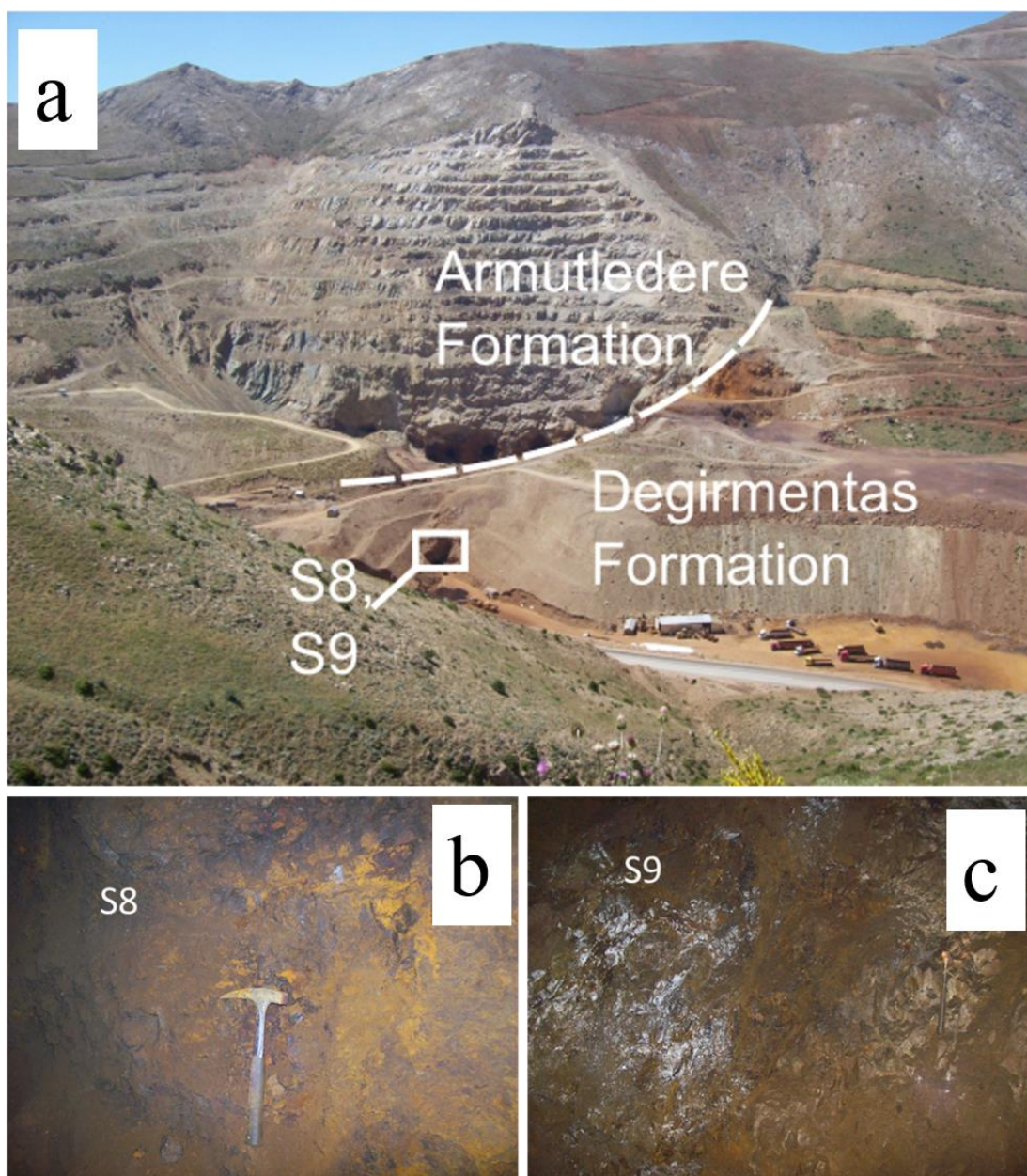


Figure S4. Photograph of the Magarabeli iron mine (A). Samples were taken from

section of the mine highlighted within the white box in image A. B) context of sample S8. C) context of sample S9.

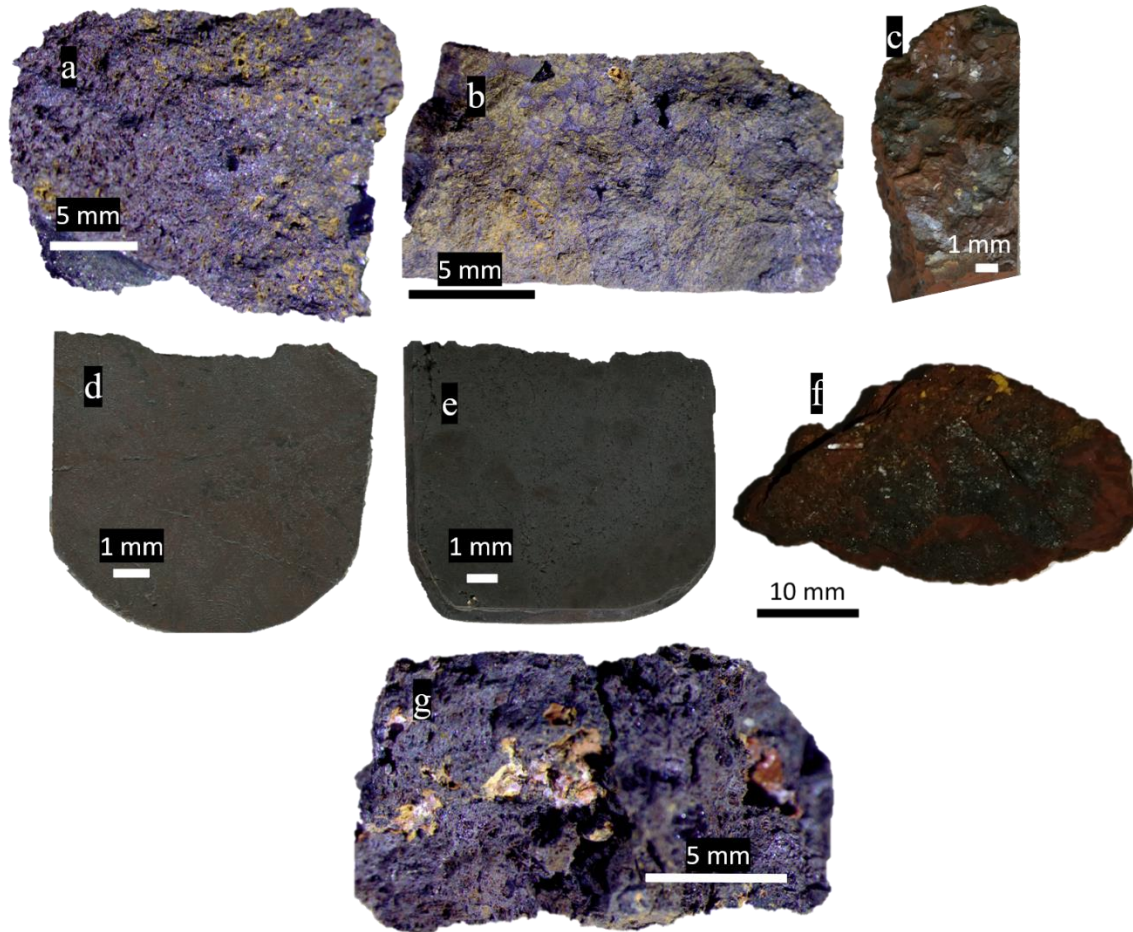


Figure S5. Images of hand samples used in this study. A) Sample S1: fresh surface of a chip liberated from larger sample. Metallic grey of goethite with friable yellow weathering evident. B) Sample S3: fresh surface of a chip liberated from larger sample. Metallic grey of goethite with friable yellow weathering evident. C) Sample S4: Representative broken chip, similar to that used for SEM analysis, showing fresher metallic grey of hematite and deeper red weathering. D) Sample S8: Broken polished block showing metallic lustre of hematite and weathered hematite/goethite red/brown patchy surface. E) Sample S9: Broken polished block showing metallic lustre of hematite/magnetite and weathered red patchy surface. F) Sample S10: Broken chip showing darker metallic lustre of hematite alongside friable weathered red and yellow

patches. G) Sample S11: fresh surface of a chip liberated from larger sample. Metallic grey of goethite with friable yellow weathering evident.

Era	Epoch	Age	Fm.	Lithology	Description
Cenozoic	Quat.		Alv.		Sand, pebble, gravel, silt
	Neogene	Miocene	Yaylacik Fm.		Angular Unconformity Conglomerate, sandstone, tuffa, volcaniclastics
Mesozoic		Cretaceous	Ophiolite + ophiolitic melange		Angular Unconformity Serpentinite, dunite, gabbro, limestone melange
		Jura.	Kizla-rsekisi Fm.		Metaconglomerate, phyllite, recrystallises limestone with iron ore
Palaeozoic		Ordovician	Armutludere Fm.		Unconformity/ tectonic contact Schist, phyllite, shales, calcshisct lenses with iron ore
		Cambrian	Degirmentas Fm.		Tectonic contact Grey, beige, off-white clays with dolomitic limestone and iron ore
		Lower	Zabuk Fm.		Tectonic contact Metasandstone/purple quartzite with pyrite
Precambrian			Emirgazi Fm.		Unconformity/ tectonic contact Graphitic shale, metasandstone, pelite, quartzite, and metavolcanics with limestones, pyrite, and uneconomic siderite

Figure S6. Stratigraphic column showing the main geological units across the Attepe ore deposit region. Adapted from Keskin (2016)

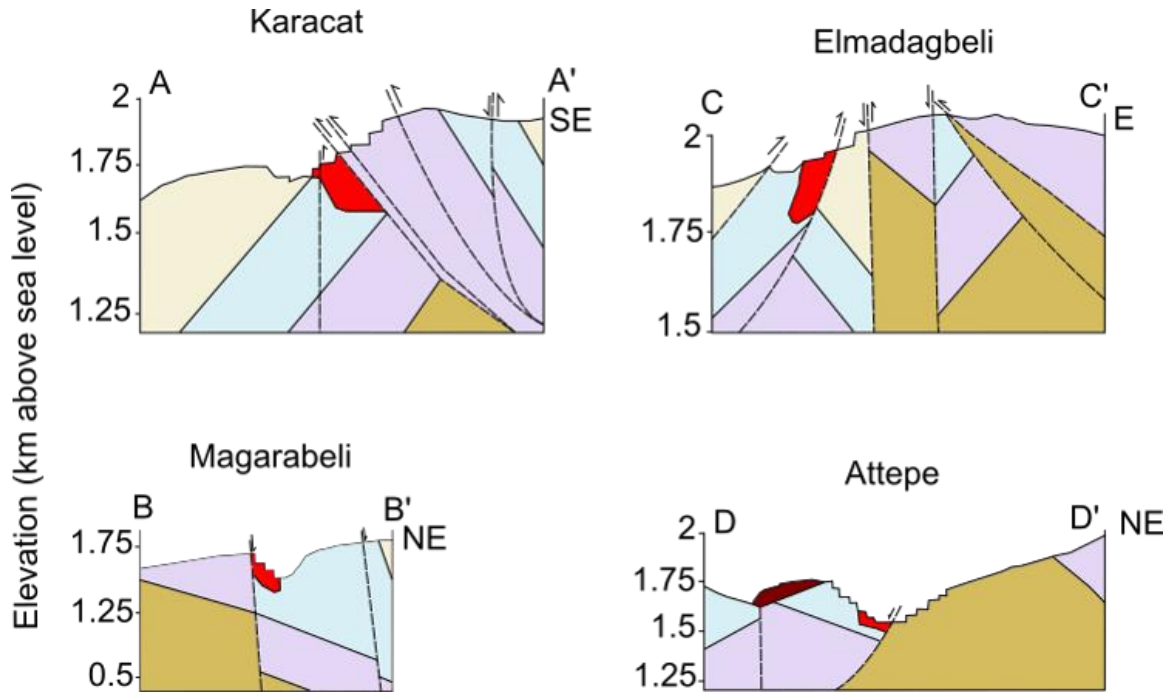


Figure S7. Cross sections of each mine showing relationship to main lithologies and faults. Cross section lines are taken from Fig. 1. C in main text. Adapted from Keskin (2016)

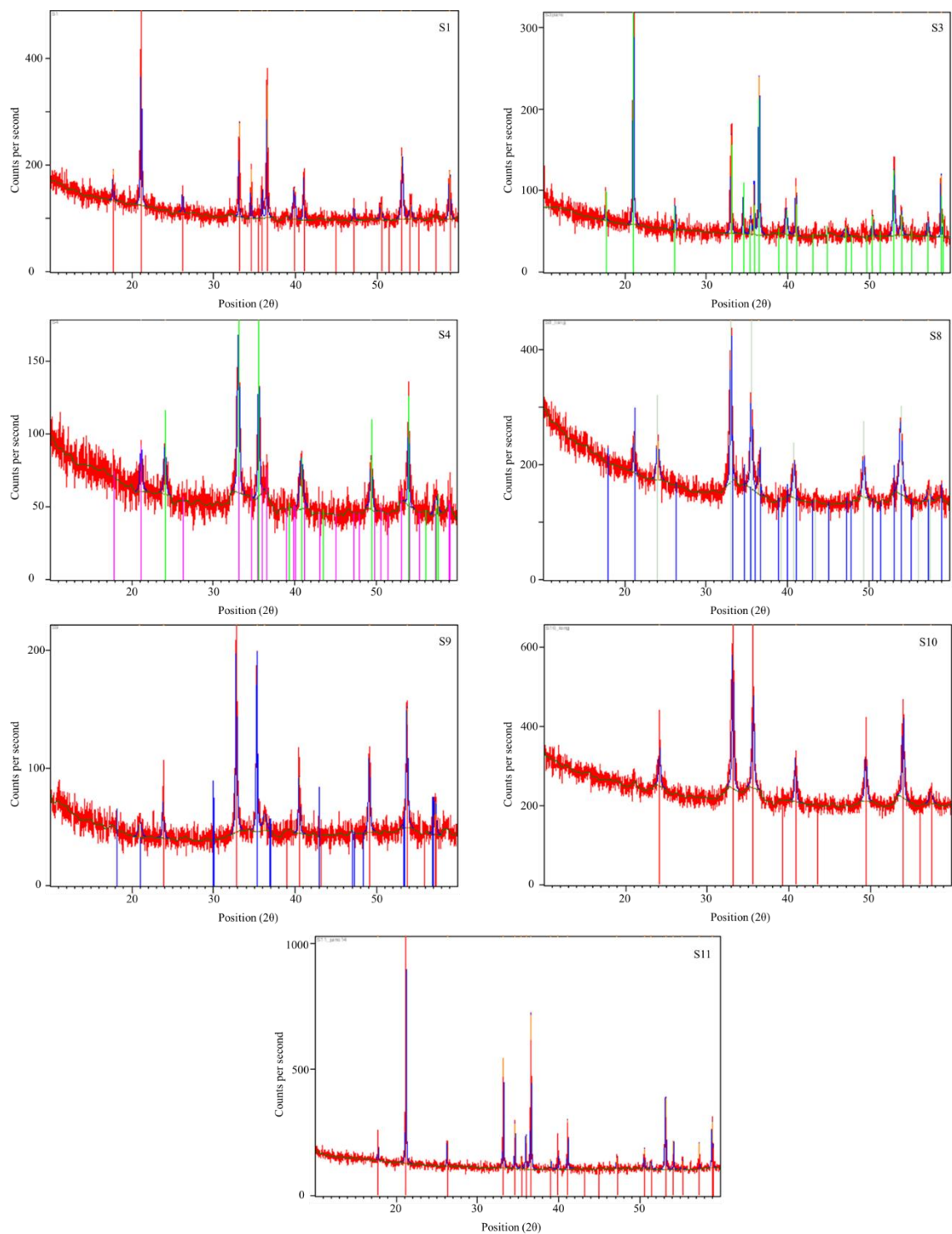


Figure S8. Diffractograms of each sample. S1: Highest intensity peak recorded at 21.10° indicative of goethite. S3: Highest intensity peak recorded at 21° indicative of goethite. S4: Highest intensity peak recorded at 31.10° indicative of hematite, with goethite a minor component recording 63 % and 32 % relative peak height (violet lines under diffractogram) and < 20 nm crystallite size. S8: Highest intensity peak recorded at 31.10° indicative of hematite, with goethite a minor component recording a 52 % relative peak

height (blue lines⁴⁵ under diffractogram) and 22 nm crystallite size. S9: Highest intensity peak recorded at 32.8θ indicative of hematite, with magnetite recording a 78 % relative peak height at 35.3θ (blue lines under diffractogram). S10: Highest intensity peak recorded at 31.1θ indicative of hematite. S11: Highest intensity peak recorded at 21.1θ indicative of goethite.

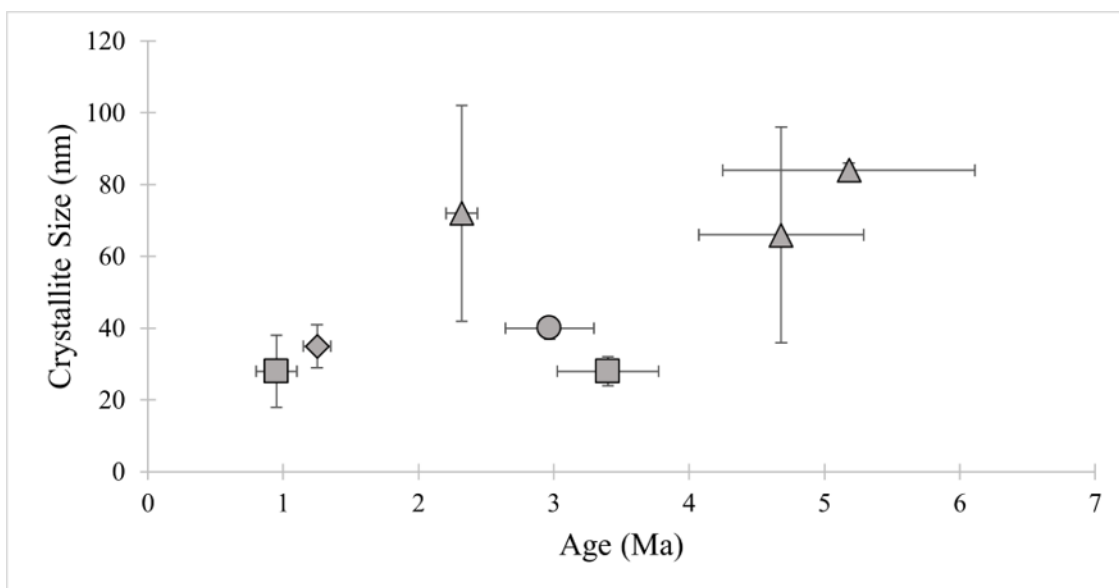


Figure S9. Age versus crystallite size and mineralogy plot. Triangle = goethite; circle = hematite/magnetite mix; square = hematite/goethite mix; rhombus = hematite

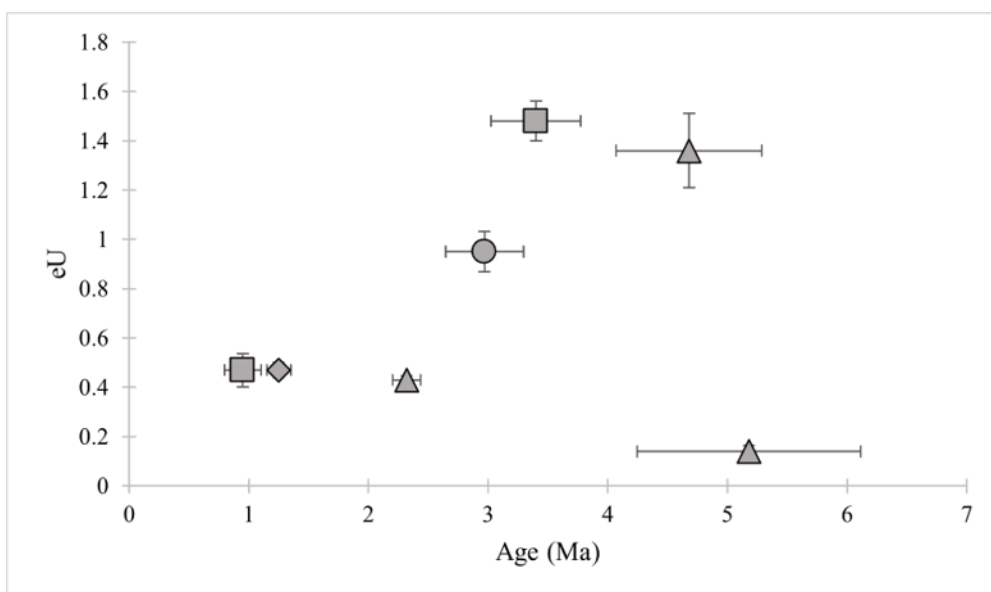


Figure S10. Age versus eU and mineralogy plot. Triangle = goethite; circle = hematite/magnetite mix; square = hematite/goethite mix; rhombus = hematite.

Sample	Mineralogy	Relative Intensity (%)	FWHM (degrees)	FWHM (radians)	Peak Position (degrees)	Peak Position (radians)	D	D average	stdev	error
S1	FeOOH	100	0.1428	0.0025	21.1	0.2	59.1	72.2	29.9	41.4%
	FeOOH	48	0.0816	0.0014	33.1	0.3	106.1			
	FeOOH	69	0.1020	0.0018	36.6	0.3	85.7			
	FeOOH	33	0.2448	0.0043	53.1	0.5	37.9			
S3	FeOOH	100	0.1428	0.0025	21.1	0.2	59.1	65.6	30.0	45.7%
	FeOOH	78	0.1632	0.0028	36.5	0.3	53.5			
	FeOOH	49	0.1428	0.0025	33.1	0.3	60.6			
	FeOOH	33	0.2448	0.0043	53.0	0.5	37.9			
	FeOOH	31	0.0816	0.0014	58.8	0.5	116.7			
S4	Fe ₂ O ₃	100	0.2856	0.0050	33.1	0.3	30.3	27.6	10.0	36.2%
	Fe ₂ O ₃	88	0.2040	0.0036	35.6	0.3	42.7			
	FeOOH	63	0.4896	0.0085	54.0	0.5	19.0			
	FeOOH	32	0.4896	0.0085	40.8	0.4	18.1			
	Fe ₂ O ₃	31	0.3264	0.0057	49.4	0.4	28.0			
S8	Fe ₂ O ₃	100	0.2856	0.0050	33.1	0.3	30.3	27.9	4.4	15.7%
	Fe ₂ O ₃	57	0.2856	0.0050	35.6	0.3	30.5			
	FeOOH	52	0.4080	0.0071	53.9	0.5	22.8			
S9	Fe ₂ O ₃	100	0.2040	0.0036	32.8	0.3	42.4	40.1	2.9	7.1%
	Fe ₃ O ₄	78	0.2040	0.0036	35.3	0.3	42.7			
	Fe ₂ O ₃	61	0.2448	0.0043	53.7	0.5	38.0			
	Fe ₂ O ₃	38	0.2448	0.0043	49.1	0.4	37.3			
S10	Fe ₂ O ₃	100	0.2244	0.0039	33.1	0.3	38.6	34.5	5.7	16.5%
	Fe ₂ O ₃	61	0.2856	0.0050	35.6	0.3	30.5			
	Fe ₂ O ₃	57	0.2448	0.0043	54.0	0.5	38.0			
S11	FeOOH	100	0.1020	0.0018	21.2	0.2	82.8	84.4	1.5	1.8%
	FeOOH	48	0.1020	0.0018	33.2	0.3	84.9			
	FeOOH	68	0.1020	0.0018	36.6	0.3	85.7			
Average D (nm)								50.3	23.3	46.2%

Scherrer equation $D = k \times \lambda / \beta (\cos\theta)$

D = crystallite size (nm)

k = Scherrer's Constant (for spherical crystallites with cubic symmetry) 0.94

λ = x-ray wavelength Cu K-alpha 1.5406; or 0.15406 Angstrom.

β = FWHM (Full Width Half Maximum in radians - peak width)

θ = peak position (radians) 0.5

Table S1. XRD diffractogram data from iron oxide/oxyhydroxide samples from the Attepe iron deposits, Turkey.